Journal of Chemical Engineering of Japan, Vol. 35, No. 10, pp. 952–962, 2002 **Research Paper**

Theoretical Analysis of Bubble Formation in a Co-Flowing Liquid

W. B. CHEN AND REGINALD B. H. TAN
Department of Chemical and Environmental Engineering, National University of Singapore, Singapore 119260

***Keywords*:** Non-Spherical Model, Bubble Formation, Liquid Flow, Co-Flowing, Bubble Axis Translation

A realistic non-spherical model for bubble formation in a co-flowing liquid is presented. In the model, an interfacial element approach is applied to describe the dynamics of bubble formation. The effect of flowing liquid velocity is modeled by a combination of the bubble axis translation and liquid pressure analysis of each interfacial element. The bubble shapes during formation are predicted reasonably well by the present model. The effects of liquid velocity, gas flow rate, nozzle radius and gas chamber volume on the bubble growth rates are studied. The model predictions are compared with the experimental data in literature and show good agreement.

Introduction

In many practical chemical processes, continuous operation is more frequently used than batch and semi-batch operations, in which not only gases but also liquids are continuously fed into a column. Therefore, bubble formation in flowing liquids is of wide interest in engineering applications.

Bubble formation in co-flowing or counter-flowing liquids under constant gas flow conditions has been investigated both experimentally and theoretically (Chuang and Goldschmidt, 1970; Sada *et al*., 1978; Takahashi *et al*., 1980; Räbiger and Vogelpohl, 1982; Fawkner *et al*., 1990; Oğuz and Prosperetti, 1993). Several spherical, pseudo-spherical and non-spherical models have been reported for bubble formation in flowing liquids. All the investigations reported that the bubble volume decreased with an increase of superficial liquid velocity.

One-stage spherical models Chuang and Goldschmidt (1970) were the first to propose a one-stage model for bubble formation at a nozzle submerged in co-flowing liquid. Their model was based on the force balance at bubble detachment. The bubble volumes were obtained from the force balance equation or its dimensionless form. Sada *et al*. (1978) observed bubble formation at a single nozzle in water flowing parallel to the nozzle. The gas flow rate and superficial liquid velocity ranged from 0.33×10^{-6} m^3/s to 36.2×10^{-6} m^3/s and from 0 m/s to 1.549 m/s, respectively. It was assumed that the total force acting on the bubble at the nozzle is the sum of the buoyancy force and the drag force. By using a modified Froude number, they obtained the dimensionless correlation of bubble size in the single bubbling regimes. Fawkner *et al*. (1990) developed a theory to explain the variation in bubble sizes obtained when a flowing liquid was pulsed into a column into which a constant flow of air was sparged through a vertical nozzle at its base. This one-stage model was based on that developed by Davidson and Schüler (1960) for bubble formation in a quiescent liquid. The bubble was assumed to be spherical at all times during its formation. The upward motion of the bubble was accounted for by superimposing the liquid motion on that obtained from a balance between the upward force due to buoyancy and the drag force due to inertia. Bubble detachment was assumed to take place when the distance between the bubble base and the nozzle center was equal to the nozzle radius. The results predicted by the model agreed well with their experimental data.

Two-stage spherical models Takahashi *et al*. (1980) observed the bubble formed in co-current, counter-current, and crosscurrent flowing liquids under a constant flow conditions. To estimate the bubble volume, a two-stage spherical model based on the model of Takahashi and Miyahara (1976) in quiescent liquid was proposed, involving an empirically formulated correlation factor. Newton's second law of motion applied both at the end of the first stage and the second stage were given to determine the bubble volume. Räbiger and Vogelpohl (1982) conducted experimental and theoretical studies on bubble formation in flowing Newtonian liquids. A two-stage model based on Ramakrishnan *et al*. (1969) in a quiescent liquid was developed to calculate the bubble volume. The correlations obtained from the model showed a good agreement for the maximum bubble pressure and the detachment of bubbles.

Received on November 25, 2001. Correspondence concerning this article should be addressed to R. B. H. Tan (E-mail address: chetanbh@nus.edu.sg).

Pseudo-spherical model Terasaka *et al*. (1999) experimentally investigated the effects of liquid velocity, nozzle diameter, gas chamber volume and gas flow rate on volumes, shapes and growth rates of bubbles formed at a nozzle submerged in a co-current upward flowing liquid. A modified pseudo-spherical model, based on that of Terasaka and Tsuge (1990) for bubble formation in a quiescent liquid, was proposed. Although the bubble volumes, bubble growth rates and shapes were well predicted by the model, this model still contained the same inadequacies present in the original model of Terasaka and Tsuge (1990), that is, the equations of motion for expansion and translation of an equivalent spherical bubble were utilized for a model of bubble formation.

Non-spherical models Oğuz and Prosperetti (1993) employed a boundary integral method to predict the bubble shapes and volumes in a flowing inviscid liquid under constant pressure in a gas chamber connected to a nozzle. The pressure in the bubble was taken to be spatially uniform, while the liquid pressure at the bubble interface was not required to be uniform and the bubble was not assumed to grow spherically. The effects of nozzle length, gas flow rate and liquid flowing velocity on the behavior of growing bubble were well predicted by the model. This model is limited to constant pressure bubbling conditions and low gas flow rates.

In this study, a realistic non-spherical model for bubble formation, which is based on interfacial element approach, is developed to predict the bubble shapes, growth rates and bubble volume and time at detachment. Model predictions are compared with the experimental results of Terasaka *et al*. (1999).

1. Model Development

Non-spherical models of bubble formation have been successful in predicting bubble formation in a quiescent liquid. In particular, the interfacial element approach employed by Marmur and Rubin (1976) and Tan and Harris (1986) has yielded good agreement with experimental results for bubble growth rate, detachment time, bubble volume at detachment and chamber pressure fluctuations. The interfacial element method was also successful in modeling of bubble formation with liquid cross-flow (Tan *et al*., 2000).

Our present theoretical model for bubble formation in a co-flowing liquid will be based on this modified interfacial element approach. Thermodynamic expressions relating the chamber and bubble pressures and the instantaneous bubble volume are solved to provide the orifice gas flow rate. The effect of a parallel flowing liquid is taken into account by combination of bubble axis translation and pressure analysis of the surrounding liquid.

1.1 Physical system and basic assumptions

The bubbling system under consideration consists a gas that is fed into a chamber with volume V_c, at a constant flow rate Q and pressure P_o. Gas flows through the single nozzle R_o into the bubble at a flow rate q. This flow is assumed to be controlled by the pressure in the chamber and that in the bubble, P_c and P_b, which are both assumed to be uniform within their volumes. A liquid flows upward at a velocity U_l parallel to the nozzle axis. The following basic assumptions are made:

(a) The bubble remains symmetrical about its vertical axis during the growth and is a volume of revolution around its vertical axis.

(b) The influence of gas and liquid viscosities at the interface is negligible.

(c) The growth of the bubble is unaffected by the presence of other bubbles.

(d) The gas is ideal and the flow is adiabatic.

(e) The upward flowing liquid is isothermal, uniform, inviscid and irrotational.

(f) There is no energy exchange or mass transfer across the gas-liquid interface.

1.2 Equations of motion

1.2.1 Interfacial element representation of the bubble interface The interfacial element approach divides the bubble interface into a number of small elements. Because of assumption (a), the three-dimensional bubble can be simply analyzed in a two-dimensional way: with virtual axial direction z^* and virtual radial direction r^* in the $r^*– z^*$ plane, which is a virtual space and does not take the co-flowing liquid velocity into account, and only one side of the bubble needs to be considered.

Figure 1(**a**) shows the axisymmetric bubble surface represented by a single curve in the $r^*– z^*$ plane, which consists of a number of small elements. The center of each element is represented by a black circle on the curve. For a specific element i, the end points of the element are the midpoints between point i and each of its two nearest neighbors on both sides.

Equations of motion are developed from force balances carried on each element. The equations are written in finite-difference form and solved numerically to obtain the instantaneous coordinates of all elements. The position of the bubble surface at each instant during its growth can be determined by the instantaneous position of each element.

1.2.2 Basic equations Figure 1(**b**) shows a three-dimensional differential element of this interface and the forces acting on it. The surface force is due to pressure difference between the gas in the bubble and the liquid, and the line forces are due to surface tension. For a static interface, these forces are in equilibrium. However, in dynamic bubble formation, the resultant of these forces is equal to the rate of change in the liquid momentum. Figure 1(b) shows also an initial differential interface element dA_0, which grows to dA af-

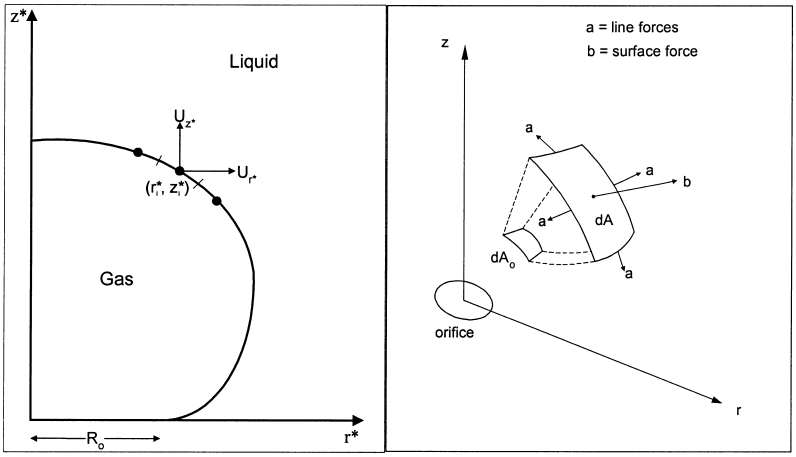

Fig. 1 (a) Two-dimensional interfacial element representation of bubble surface: (b) Forces acting on an interfacial element, in cylindrical coordinate

ter time t, and the volume of liquid displaced by the differential element during this time period. To avoid the extremely complicated solution of the Navier-Stokes equations for the motion of liquid, liquid momentum can be calculated using the inertial mass and the velocity of the interface element:

$$\tilde{F}_i = \frac{d}{dt}\left(\tilde{U}_i \overline{m}_i\right) \tag{1}$$

where $\overline{m}_i$ is the added mass of liquid accelerated by the motion of the interface element at a velocity $\tilde{U}_i$, and

$$\overline{m}_i = \left(\alpha\rho_\mathrm{l} + \rho_\mathrm{b}\right)V_i \tag{2}$$

where α is the theoretical added mass coefficient [= 0.6875], ρ_b, ρ_l are the density of bubble and surrounding liquid, respectively. V_i is the volume of liquid displaced by the element since the beginning of its movement.

Resolving Eq. (1) to give coordinates of specified differential interface element in space as a function of time, considering unit angle of revolution, κ about the bubble axis, we obtain a set of differential equations of motion in cylindrical coordinates:

$$r_i^* \Delta P_i dr_i^* - \sigma d\left(r_i^* \sin\beta_i\right) = \frac{d}{dt}\left(U_{z^*}\overline{m}\right)_i \tag{3}$$

$$r_i^* \Delta P_i dz_i^* - \sigma\left[d\left(r_i^* \cos\beta_i\right) - \frac{dz_i^*}{\sin\beta_i}\right] = \frac{d}{dt}\left(U_{r^*}\overline{m}\right)_i \tag{4}$$

where r^*, z^* are virtual radial coordinate from the axis of the bubble and axial coordinate from nozzle horizontal level respectively, as shown in Fig. 1(a), ΔP_i is the pressure difference between bubble pressure P_b and the liquid pressure P_l at each interface element. β is an angle defined by:

$$\beta = \tan^{-1}\frac{\partial z^*}{\partial r^*} \tag{5}$$

To account for a parallel flowing liquid with upward velocity U_l, the apparent vertical translation of each interface element, dz^*/dt, is defined relative to the uniform liquid velocity U_l. The relationship between the virtual coordinates r^*, z^* and the fixed cylindrical coordinates r, z yields (Terasaka *et al.*, 1999):

$$\frac{dz^*}{dt} = \frac{dz}{dt} - U_\mathrm{l} \tag{6}$$

and

$$\frac{dr^*}{dt} = \frac{dr}{dt} \tag{7}$$

1.3 Thermodynamics of the system

The equations of motion are based on a differential force balance at the gas-liquid interface. This force balance involves the pressure difference between the gas within the bubble and the liquid. Hence, calculation of the instantaneous pressure within the bubble and the pressure distribution around the surrounding liquid are required.

The pressure within the bubble is determined by its thermodynamic relation to the pressure in the gas chamber and the flow rate through the nozzle. According to the basic assumptions made on the physical sys-

tem, the thermodynamic equations describing the bubbling system are derived as bellow.

A mass balance on the chamber yields

$$V_c \frac{d\rho_c}{dt} = \rho_a Q - \rho_c q \tag{8}$$

where ρ_a and ρ_c are the gas densities at supply and chamber conditions, respectively.

Similarly, applying mass balance to the gas within the bubble,

$$\frac{d\rho_b V_b}{dt} = \rho_c q \tag{9}$$

or the molar change of gas within the bubble can be expressed as

$$dn = dn_{in} - dn_{out}, \quad \text{and} \quad dn_{out} = 0 \tag{10}$$

Applying open system energy balance (or the first law of thermodynamics for an open system) to the gas with the bubble, the internal energy change of gas within the bubble, dE_b, can be expressed in terms of the heat interaction across the gas-liquid interface, $d\Theta$, work interaction across gas-liquid interface, dW, and energy balance due to a non steady flow (the last four terms in the right-hand side of Eq. (11)),

$$dE_b = d\Theta + dW + \left[\left(h_{in} dn_{in} + dE_{k,in}\right) - \left(h_{out} dn_{out} + dE_{in,out}\right)\right] \tag{11}$$

Here

$$dE_b = n de_v + e_v dn = n_{in} de_v + e_v dn_{in} \tag{12}$$

and e_v is molar internal energy of gas within a bubble.

As we assume that there is no heat transfer across the gas-liquid interface,

$$d\Theta = 0 \tag{13}$$

$$dW = -P_b dV_b \tag{14}$$

The contribution of the kinetic energy of gas through the orifice is taken into account in the equation. This change in kinetic energy is assumed to arise from the trapping of the upward flowing gas by the bubble envelope, and may affect the bubble pressure significantly due to the small bubble volume. This change of the kinetic energy may be expressed as:

$$dE_{k,in} = \frac{\rho_b}{2}\left(\frac{q}{a_o}\right)^2 q dt \tag{15}$$

$$dE_{k,out} = 0 \tag{16}$$

where a_o is the cross-sectional area of the orifice.

Substituting Eqs. (12)–(16) into Eq. (11), it follows that

$$n_{in} C_v dT + P_b dV = R_g T dn_{in} + \frac{\rho_v}{2}\left(\frac{q}{a_o}\right)^2 q dt \tag{17}$$

where C_v is constant-volume heat capacities.

Rewriting Eq. (17) together with an ideal gas law equation

$$P_b V_b = n R_g T \tag{18}$$

The pressure change of the gas within the bubble is obtained

$$\frac{dP_b}{dt} = \frac{1}{V_b}\left[\gamma \rho_c q + (\gamma - 1)\frac{\rho_c q^3}{2a_o^2} - \gamma P_b \frac{dV_b}{dt}\right] \tag{19}$$

where γ is adiabatic gas exponent.

A similar derivation of pressure change within the chamber was obtained

$$\frac{dP_c}{dt} = \frac{\gamma}{V_c}\left(P_a Q - P_c q\right) \tag{20}$$

In this case, the kinetic energy change between inflow and outflow is taken to be negligible. This can be justified by the fact that the effect of gas kinetic energy on chamber pressure is small when the chamber is large. If the chamber volume is small, the gas flow rates into the chamber and out through the orifice are approximately the same. Hence, the net change of gas kinetic energy is close to zero.

The pressure drop through a nozzle can be described as follows (Terasaka, *et al.*, 1999)

$$P_c - P_b = k_1 q + k_2 q^2 \tag{21}$$

where k_1 and k_2 are experimentally obtained.

Equations (8), (9), (19), (20) and (21) make up a set of simultaneous differential equations and can be solved to obtain P_b, P_c, ρ_b, ρ_c, and q via an explicit finite time-difference method.

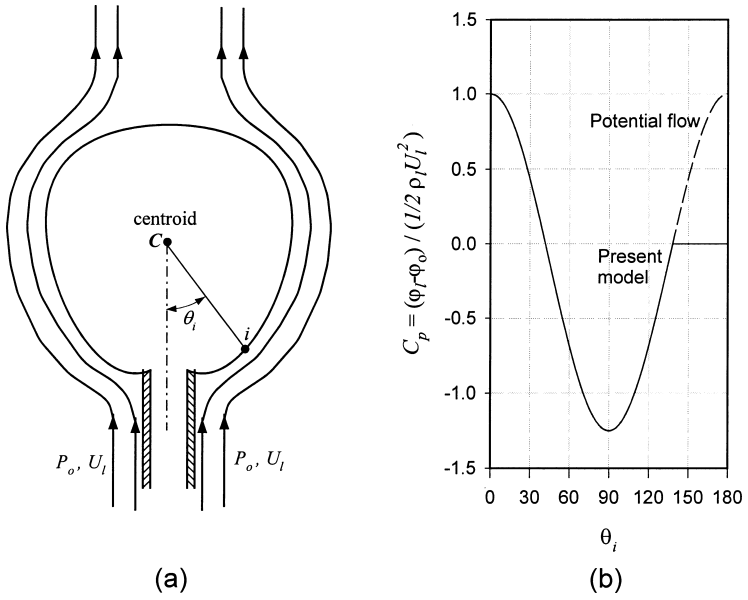

Fig. 2 Analysis of liquid pressure distribution: (a) geometry for estimation of liquid pressure distribution, (b) distribution of dimensionless modified pressure: (---) potential flow for spheres and (—) approximation for fluid spheres

1.4 Calculation of liquid pressure

The effect of the parallel liquid flow (velocity U_l) is estimated via the liquid pressure distribution at the bubble interface as shown in **Fig. 2**. The centroid, C, of the bubble envelope is located by the expression:

$$z_c = \frac{\int_1^n z_i dS_i}{S} \tag{22}$$

For each time step, the angle θ_i for each interface element i is defined as shown in Fig. 2(a). Figure 2(b) shows the values of the pressure coefficient C_p for a steady flow around a fluid sphere (Hamielec *et al.*, 1967). The authors provided the steady state solutions of the Navier-Stokes equations for flows around circulating fluid spheres by using finite-difference methods. Their results showed that the potential flow solution provided a good approximation at the front part of a bubble (Clift *et al.*, 1978). The dashed line is the analytical solution for an ideal potential flow, while the solid line was used in the present model as a close approximation to Hamielec *et al.*, (1967) solution. In the present model, C_p is estimated as follows:

$$C_p = 1 - \frac{9}{4}\sin^2\theta_i, \qquad 0 \le \theta_i \le 138.2° \tag{23a}$$

$$C_p = 0, \qquad \theta_i > 138.2° \tag{23b}$$

Thus, liquid pressure distribution on the surface of a bubble can be calculated:

$$\varphi_l = \varphi_o + \frac{1}{2}\rho_l U_l^2 C_p \tag{24}$$

where φ_l and φ_o are non-gravitational pressures with reference to the orifice,

$$\varphi_l = P_l + \rho_l g z \tag{25}$$

$$\varphi_o = P_o \tag{26}$$

Therefore, liquid pressure distribution can be computed by:

$$P_l = P_o + \frac{1}{2}\rho_l U_l^2 C_p - \rho_l g z \tag{27}$$

where P_o is absolute liquid pressure at the orifice,

$$P_o = P_s + \rho_l g h - \frac{1}{2}\rho_l U_l^2 \tag{28}$$

and P_s is system pressure above the bulk liquid.

2. Numerical Solution

2.1 Initial and boundary conditions

The bubble is initially assumed to be a hemisphere of radius equal to the nozzle radius, and its interface is represented by N equally spaced points. Each point represents a mid-point of an interfacial element.

The initial pressures in the bubble and chamber are both assumed to be the sum of hydrostatic pressure

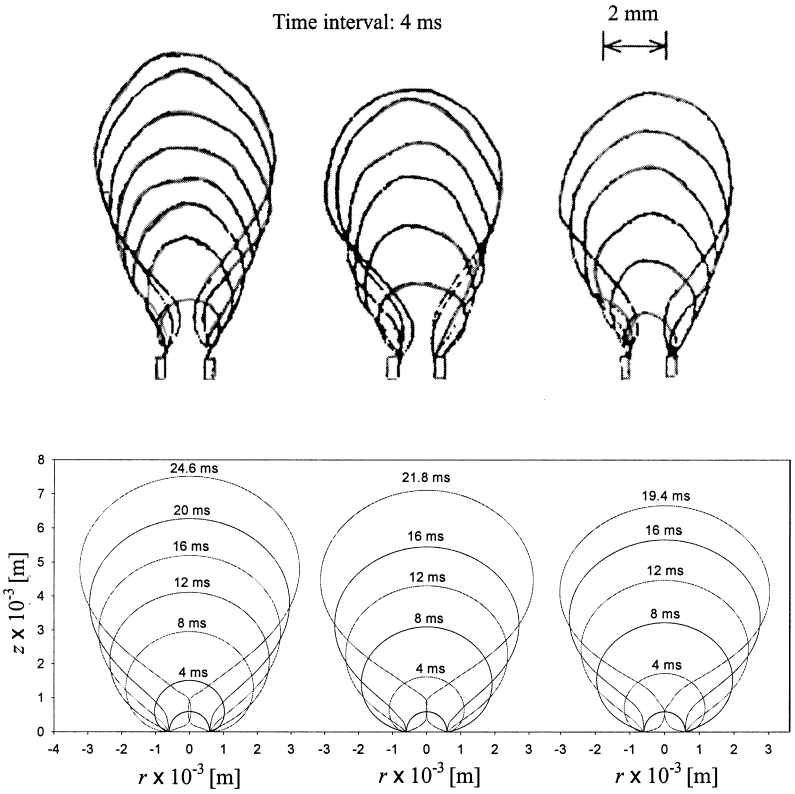

Fig. 3 Effect of co-flowing liquid velocity on the bubble shapes during formation for experimental conditions: N_2/Water, $Q = 5.11 \times 10^{-6}$ m^3/s, $R_0 = 0.595 \times 10^{-3}$ m, $V_c = 49.7 \times 10^{-6}$ m^3, $U_1 = 8.67 \times 10^{-2}$, 13.0×10^{-2}, 16.5×10^{-2} m/s, respectively (from left to right). Experimental photographs are from Terasaka *et al.* (1999)

at the nozzle and the excess pressure due to surface tension

$$P_c(t=0) = P_b(t=0) = P_o + \frac{2\sigma}{R_0} \tag{29}$$

Hence, the orifice flow rate is assumed to be zero initially,

$$q(t=0) = 0 \tag{30}$$

2.2 Computational procedure

After initialization and time increment, the new coordinates of each element are computed by solving differential equations of motion via an explicit finite time-difference method (Refer to Appendix). The new bubble volume at time t is then obtained by a numerical integration of the new coordinates of each element, and used to evaluate the new chamber and bubble pressures. The pressure of surrounding liquid is evaluated by Eq. (27). When the radial distance between an element on the neck and the bubble vertical axis is reduced to zero, bubble detaches.

The bubble interface is divided initially by 50 points, which is sufficient to adequately represent the bubble shape. Since growth is non-spherical, some points on the bubble surface may tend to bunch together while others tend to move further apart during the course of the computation. Non-uniform point spacing is undesirable since excessively large spacing between elements results in an inaccurate representation of the bubble surface while bunching of element points unnecessary increases computation time. This problem is overcome by the introduction of a simple subroutine which inserts additional points when the spacing between elements become too large, and deletes points if point spacing falls within a specified range.

3. Results and Discussion

In this section, the model predictions of single bubble formation in co-flowing liquid are compared with the experimental observations by Terasaka *et al.* (1999). The following equipment variables are input to the model: orifice radius, gas chamber volume. The system variables are: gas-liquid interfacial surface tension, density of liquid, density of gas, and the adiabatic constant for the gas. The operating variables are: system pressure, gas flow rate, co-flowing liquid velocity, and liquid height above the nozzle. The experimental measured parameters k_1 and k_2 for different nozzles are obtained from Terasaka *et al.* (1999).

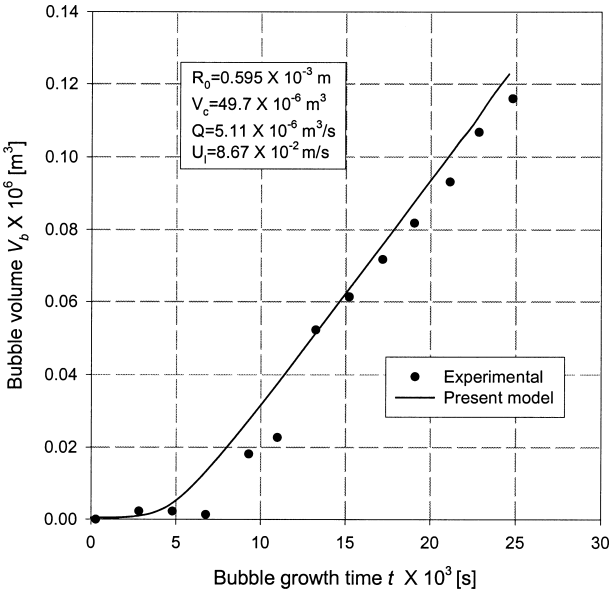

Fig. 4 Bubble growth rates in co-flowing liquid for bubble formation at conditions: N_2/Water, $Q = 5.11 \times 10^{-6}$ m^3/s, $R_0 = 0.595 \times 10^{-3}$ m, $V_c = 49.7 \times 10^{-6}$ m^3, $U_l = 8.67 \times 10^{-2}$. Experimental data from Terasaka *et al.* (1999)

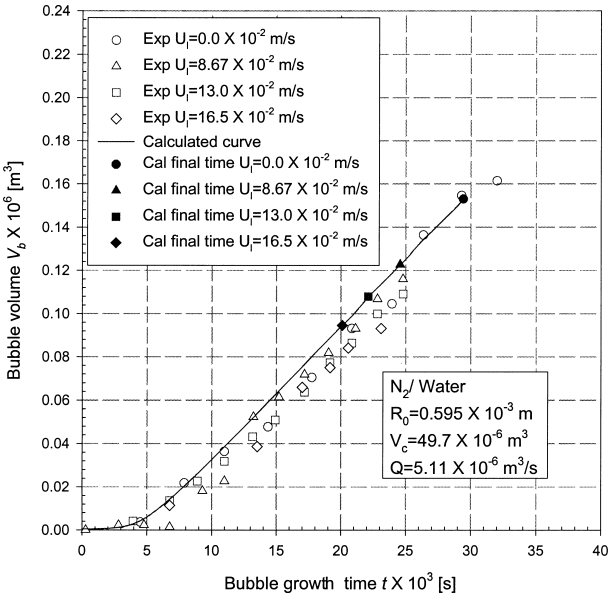

Fig. 5 Effect of co-flowing liquid velocity on the bubble growth rates. Experimental data from Terasaka *et al.* (1999)

3.1 Bubble shapes during formation

Figure 3 shows the effect of co-flowing liquid velocity on the bubble shapes during formation and detachment time. The conditions for these runs are based on the following conditions: System = N_2/Water, System pressure = atmospheric, $Q = 5.11 \times 10^{-6}$ m^3/s, $R_0 = 0.595 \times 10^{-3}$ m, $V_c = 49.7 \times 10^{-6}$ m^3, and $U_l = 8.67 \times 10^{-2}$ m/s, 13.0×10^{-2} m/s and 16.5×10^{-2} m/s, respectively, corresponding to an experimental study by Terasaka *et al.* (1999). The bubble shapes at any liquid flow velocity within the range of our study are not considerably different, and the detachment time for bubble growth decreases with an increase of co-flowing liquid velocity, which agrees very well with the experimental observations.

In Fig. 3, the time interval between two consecutive contours is 4 ms, and the final shape shows neck closure and hence detachment. These sequences clearly show that the bubbles are approximately spherical only in the early stages of formation, eventually becoming noticeably non-spherical and detaching naturally when the neck closes. The computed bubble shapes by the present model agree approximately with the shapes photographed by a high-speed video camera by Terasaka *et al.* (1999).

For large gas flow rates, gas flow velocity into a bubble increases, and the frequency of bubble generation also increases. A significant pressure wake is caused by the previous rising bubble, so that the bubble shapes may become slightly elongated along the axis. In our present model, the effect of the presence of others bubbles is not taken into account. Hence the computed bubble shapes appear to be more rounded and less sharpened at the top. However, the general agreement on both shape and size is reasonable.

3.2 Bubble growth rates

Figure 4 shows the bubble volume computed at various times during the formation period. The conditions for this run are corresponding to Fig. 3 with $U_l = 8.67 \times 10^{-2}$ m/s, and a comparison is made with bubble volume experimentally obtained by Terasaka *et al.* (1999). The figure indicates that the results computed by the present model correlate well with the experimental data.

3.2.1 Effect of liquid velocity **Figure 5** shows the bubble growth rates for several values of co-flowing liquid velocity. The conditions for these runs are corresponding to Fig. 3. The symbols represent the bubble volume and time at detachment for different liquid flow velocities. Clearly, the instantaneous bubble growth rate is virtually unaffected by the co-flowing liquid velocity. The main effect of liquid flow velocity is to affect the detachment time, and thereby the bubble volume at detachment. With increasing liquid flow velocity, the bubble is predicted to detach earlier and the bubble volume at detachment is consequently smaller. These results agree with the experimental observations and trends reported by Terasaka *et al.* (1999).

3.2.2 Effect of gas flow rate **Figure 6** shows the effect of gas flow rate on bubble growth rates for the conditions: System = N_2/Water, System pressure = atmospheric, $R_0 = 0.595 \times 10^{-3}$ m, $V_c = 49.7 \times 10^{-6}$ m^3, $U_l = 13.0 \times 10^{-2}$ m/s, corresponding to the experimental run in Terasaka *et al.* (1999). The bubble has a longer

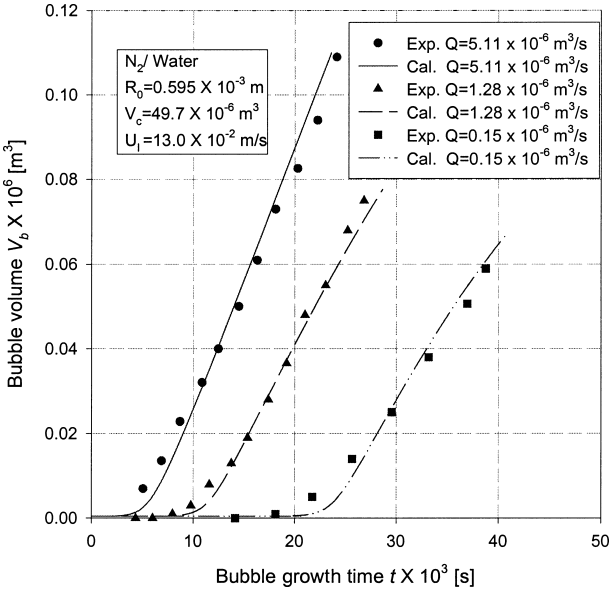

Fig. 6 Effect of gas flow rate on bubble growth rate in co-flowing liquid. Exoerimental data from Terasaka *et al*. (1999)

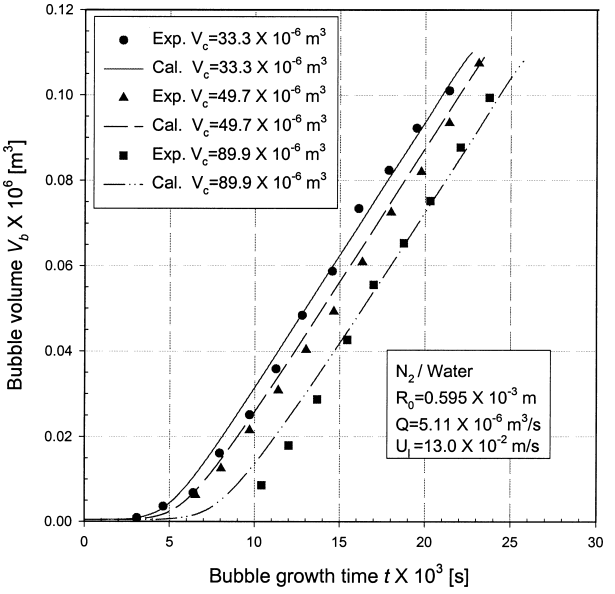

Fig. 8 Effect of gas chamber volume on bubble growth rate in co-flowing liquid. Experimental data from Terasaka *et al*. (1999)

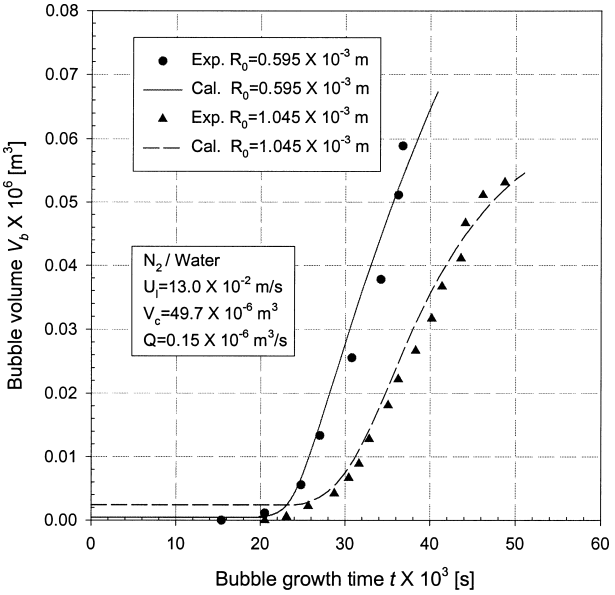

Fig. 7 Effect of nozzle radius on bubble growth rate in co-flowing liquid. Experimental data from Terasaka *et al*. (1999)

growth time and the final bubble volume is smaller when the injected gas flow rate is lower as expected empirically. This trend is also observed experimentally for single bubble formation in a quiescent liquid. It can be noted again that the model predictions match the experimental data rather well.

3.2.3 Effect of nozzle radius **Figure 7** shows the effect of nozzle radius on bubble growth rates for the conditions: System = N_2/Water, System pressure = atmospheric, $Q = 0.15 \times 10^{-6}$ m^3/s, $V_c = 49.7 \times 10^{-6}$ m^3, $U_l = 13.0 \times 10^{-2}$ m/s, corresponding to the experimental run in Terasaka *et al*. (1999). When the nozzle radius is larger, the rate of the increase of bubble volume is slower. An increase in nozzle radius causes the reduction of a pressure drop through the nozzle, which means the driving force for bubble formation is reduced. Therefore, bubble growth rate is slower in the case of larger nozzle radius.

3.2.4 Effect of gas chamber volume The effect of gas chamber volume on bubble growth rate is shown in **Fig. 8** for experimental conditions: System = N_2/Water, System pressure = atmospheric, $Q = 5.11 \times 10^{-6}$ m^3/s, $R_0 = 0.595 \times 10^{-3}$ m, $U_l = 8.67 \times 10^{-2}$ m/s, corresponding to experimental run in Terasaka *et al*. (1999).

The bubble begins to expand earlier in the case of smaller gas chamber volume. While, the final bubble volumes at detachment are almost same in this conditions.

3.3 Variation of bubble volume with liquid flow velocity and gas flow rate

Figure 9 shows the variation of bubble departure radius with co-flowing velocity for the conditions: System = N_2/Water, System pressure = atmospheric, $R_0 = 0.595 \times 10^{-3}$ m, $V_c = 49.7 \times 10^{-6}$ m^3, $Q = 0.138 \times 10^{-6}$, 1.28×10^{-6}, 5.11×10^{-6} m^3/s. Simulated results are compared with the experimental data available (Terasaka *et al*., 1999) for the influence of co-flowing liquid velocity on bubble volumes at the three values of gas flow rate. For all gas flow rates studied, bubble volume at detachment decreases with the increase of liquid flow velocity. It can be seen that the model predictions follow the experimental trends rather well.

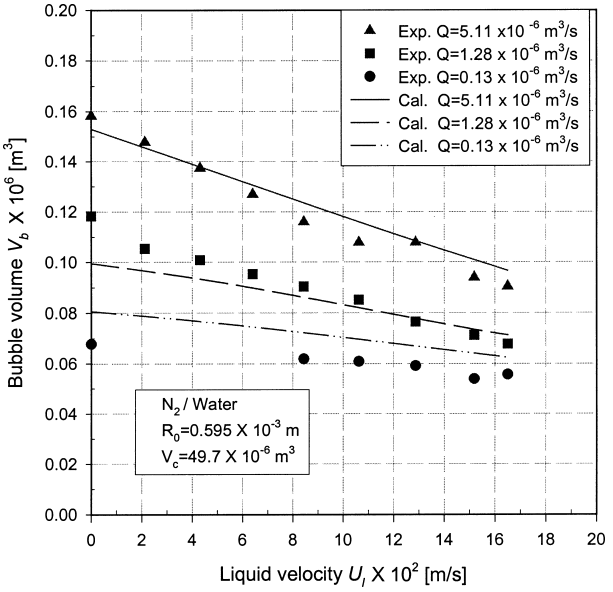

Fig. 9 Variation of bubble volume at detachment with co-flowing liquid velocity. Experimental data from Terasaka *et al.* (1999)

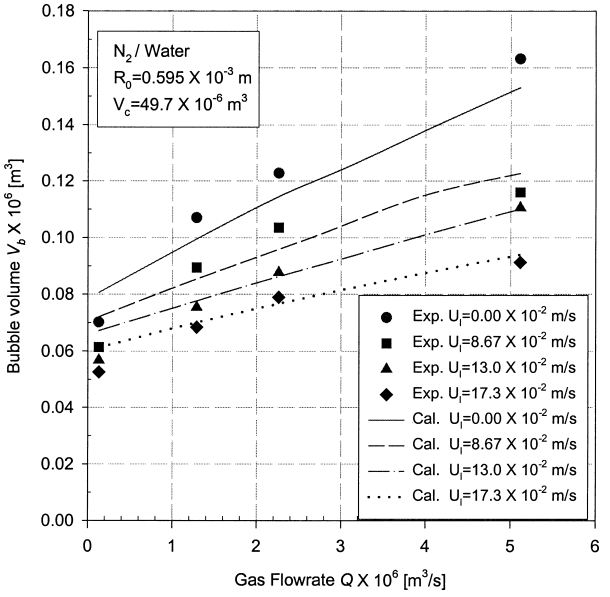

Fig. 10 Variation of bubble volume at detachment with gas flow rate. Experimental data from Terasaka *et al.* (1999)

The variation of bubble volume at detachment with gas flow rate is shown in **Fig. 10**; the conditions are: System = N_2/Water, System pressure = atmospheric, $R_0 = 0.595 \times 10^{-3}$ m, $V_c = 49.7 \times 10^{-6}$ m^3, $U_l = 0$, 8.67×10^{-2}, 13.0×10^{-2}, 17.3×10^{-2} m/s. At a constant liquid flow velocity, bubble volume at detachment increases when the gas flow rate increases. It can be noted again that our model predictions match the experimental trends closely.

Conclusions

In this paper, a non-spherical model for bubble formation in co-flowing liquid has been developed. The basic concepts and equations of the interfacial element method, which is applied to describe the dynamics of bubble formation, are discussed in details. Thermodynamics expressions of the bubbling system are solved together with the equation of a pressure drop through a nozzle to obtain the gas flow rate through the nozzle and the pressure of gas within the bubble. The effect of a parallel flowing liquid is taken into account by pressure analysis of surrounding liquid. Model predictions are compared with the experimental results available in literature for different conditions of liquid flow velocity, gas flow rate, nozzle radius and gas chamber volume. Bubble shapes, bubble growth rates and the variation of bubble volume with liquid flow velocity and gas flow rate are presented. The simulated results agree well with the experimental data of Terasaka *et al.* (1999).

Appendix: Finite difference forms of equations of motion

Equations (3) and (4) involve differentiation with respect to time t and virtual space. In order to solve these simultaneous differential equations of motion for each element, these equations are rewritten to be with respect to time t and fixed space, then expressed as finite difference forms.

The relationship between the variables with respect to virtual and fixed spaces is as follows:

$$U_{r^*} = \frac{dr^*}{dt} = \frac{dr}{dt} \tag{A.1}$$

$$U_{z^*} = \frac{dz^*}{dt} = \frac{dz}{dt} - U_l \tag{A.2}$$

$$\tan\theta = \frac{dz^*}{dr^*} = \frac{dz - U_l dt}{dr} \tag{A.3}$$

$$\sin\theta = \frac{dz - U_l dt}{\sqrt{(dz - U_l dt)^2 + (dr)^2}} \tag{A.4}$$

$$\cos\theta = \frac{dr}{\sqrt{(dz - U_l dt)^2 + (dr)^2}} \tag{A.5}$$

Substituting the above expressions into Eqs. (3) and (4),

$$r_i \Delta P_i dr_i - \sigma\, d(r_i \sin\beta_i) = \frac{d}{dt}\left(U_{z^*}\overline{m}\right)_i \tag{A.6}$$

$$r_i \Delta P_i (dz_i - U_l dt) + \sigma\left[d(r_i\cos\beta_i) - \sqrt{(dz_i - U_l dt)^2 + (dr_i)^2}\right] = \frac{d}{dt}\left(U_{r^*}\overline{m}\right)_i \tag{A.7}$$

Applying the differencing formula as follows:

$$U_z = \left(\frac{dz}{dt}\right)_i = \left(\frac{z - z'}{\Delta t}\right)_i, \text{ etc.} \tag{A.8}$$

$$z = \frac{z_i + z_{i-1}}{2} \tag{A.9}$$

where the superscript $'$ refers to the position at time $t - \Delta t$, and $''$ denotes the position at time $t - 2\Delta t$. Subscript i denotes element i on the bubble interface, starting from the top of the bubble.

Finally, converting Eqs. (A.6) and (A.7) to finite difference form with respect to fixed space:

$$\left\{\frac{1}{8}\Delta P_i\left[\left(r_{i+1} + r_i\right)^2 - \left(r_i + r_{i-1}\right)\right]^2 - \sigma\left[\frac{r_{i+1} + r_i}{2}\sin\theta_{i+1} - \frac{r_i + r_{i-1}}{2}\sin\theta_i\right]\right\}' = \frac{\overline{m}_i\left(z_i - z_i'\right) - \overline{m}_i'\left(z_i' - z_i''\right)}{\Delta t^2} - \frac{\overline{m}_i U_1}{\Delta t} + \frac{\overline{m}_i' U_1}{\Delta t} \tag{A.10}$$

$$\left\{r_i P_i\left(\frac{z_{i-1} - z_{i+1}}{2} - U_1\Delta t\right) + \sigma\left[\left(\frac{r_i + r_{i+1}}{2}\cos\theta_{i+1} - \frac{r_i + r_{i-1}}{2}\cos\theta_i\right) - \sqrt{\left(\frac{r_{i+1} + r_{i-1}}{2}\right)^2 + \left(\frac{z_{i+1} - z_{i-1}}{2} - U_1\Delta t\right)^2}\right]\right\}' = \frac{\overline{m}_i\left(r_i - r_i'\right) - \overline{m}'\left(r_i' - r_i''\right)}{\Delta t^2} \tag{A.11}$$

Equations (A.10) and (A.11) are arranged to yield explicit expressions for fixes position of element i

$$z_i = z_i' + \frac{\overline{m}_i'}{\overline{m}_i}\left(z_i' - z_i''\right) + \frac{\Delta t^2}{\overline{m}_i}\left(L_1 + \frac{\overline{m}_i U_1}{\Delta t} - \frac{\overline{m}_i' U_1}{\Delta t}\right) \tag{A.12}$$

$$r_i = r_i' + \frac{\overline{m}_i'}{\overline{m}_i}\left(r_i' - r_i''\right) + \frac{\Delta t^2}{\overline{m}_i} L_2 \tag{A.13}$$

where L_1 and L_2 are the left-hand-sides of Eqs. (A.10) and (A.11), respectively.

Equations (A.12) and (A.13) together with Eq. (2) can be solved to obtained three unknowns: r_i, z_i and m_i. Since m_i is itself computed from r_i and z_i, an iterative procedure is required.

Nomenclature

A	=	bubble surface shown in Fig. 1(b)	[m^2]
A_0	=	initial bubble surface shown in Fig. 1(b)	[m^2]
a_0	=	cross-sectional area of the orifice	[m^2]
C	=	centroid point of bubble envelope	
C_p	=	pressure coefficient defined in Eq. (23) and Fig. 2(b)	[—]
C_v	=	constant-volume heat capacities	[J/(mol·K)]
E_b	=	internal energy of gas within bubble	[J]
e_v	=	molar internal energy of gas within bubble	[J/mol]
$\tilde{F}_i$	=	total force acting on interfacial element i	[N]
g	=	acceleration due to gravity	[m/s^2]
h	=	height of liquid above the orifice (nozzle)	[m]
k_1	=	factor defined by Eq. (21)	[Pa·s/m^3]
k_2	=	factor defined by Eq. (21)	[Pa·s^2/m^6]
$\overline{m}_i$	=	added mass of interfacial element i	[kg]
n	=	molar number of gas within bubble	[mol]
n_{in}	=	molar number of gas injected into bubble	[mol]
P_a	=	gas pressure at inlet to chamber	[Pa]
P_b	=	pressure of gas within bubble	[Pa]
P_c	=	pressure of gas in chamber	[Pa]
P_l	=	pressure of surrounding liquid	[Pa]
P_o	=	liquid pressure at infinity	[Pa]
P_s	=	system pressure above the bulk liquid	[Pa]
Q	=	gas flow rate into chamber	[m^3/s]
q	=	gas flow rate through orifice (or nozzle)	[m^3/s]
R_o	=	orifice (or nozzle) radius	[m]
R_g	=	gas constant	[J/(mol·K)]
r	=	true radial coordinate with respect to the true vertical	[m]
r^*	=	virtual cylindrical radial coordinate from axis of bubble	[m]
t	=	bubble growth time	[s]
$\tilde{U}_i$	=	velocity of interfacial element i	[m/s]
U_l	=	liquid co-flow or cross-flow velocity	[m/s]
U_{r^*}	=	horizontal velocity of element based on virtual coordinate	[m/s]
U_{z^*}	=	vertical velocity of element based on virtual coordinate	[m/s]
V_b	=	bubble volume at any instant	[m^3]
V_c	=	gas chamber volume	[m^3]
V_i	=	volume of liquid displaced by the element i since the beginning of its movement	[m^3]
W	=	work interaction across gas-liquid interface	[J]
z	=	true axial coordinate with respect to orifice (nozzle) horizontal level	[m]
z^*	=	virtual axial coordinate from orifice (nozzle) horizontal level	[m]
α	=	added mass coefficient	[—]
β	=	angle defined in Eq. (5)	
γ	=	adiabatic gas constant	[—]
ΔP	=	pressure difference between the bubble pressure P_b and the liquid pressure P_l	[Pa]
ρ_a	=	gas density at supply	[kg/m^3]
ρ_b	=	density of vapor inside bubble	[kg/m^3]
ρ_c	=	density of vapor inside chamber	[kg/m^3]
ρ_l	=	density of surrounding liquid	[kg/m^3]
σ	=	surface tension	[N/m]
φ_l	=	non-gravitational liquid pressure on bubble surface	[Pa]
φ_o	=	non-gravitational liquid pressure at infinity	[Pa]
Θ	=	heat interaction across gas-liquid interface	[J]

Literature Cited

Chuang, S. C. and V. W. Goldschmidt; "Bubble Formation Due to a Submerged Capillary Tube in Quiescent and Coflowing Streams," *Trans. ASME, J. Basic Eng.*, **92**, 705–711 (1970)

Clift, R., J. R. Grace and M. E. Weber; Bubbles, Drops, and Particles, Academic Press, New York, USA (1978)

Davidson, J. F. and B. O. G. Schüler; "Bubble Formation at an Orifice in an Inviscid Liquid," *Trans. Instn. Chem. Engrs.*, **38**, 335–352 (1960)

Fawkner, R. D., P. P. Kluth and J. S. Dennis; "Bubble Formation at Orifices in Pulsed, Flowing Liquids," *Trans. Instn. Chem. Engrs.*, **68**, 69–73 (1990)

Hamielec, A. E., A. I. Johnson and W. T. Houghton; "Numerical Solution of the Navier-Stokes Equation for Flow Past Spheres: Part II. Viscous Flow around Circulating Spheres of Low Viscosity," *AIChE J.*, **13**, 220–224 (1967)

Marmur, A. and E. Rubin; "A Theoretical Model for Bubble Formation at an Orifice Submerged in an Inviscid Liquid," *Chem. Eng. Sci.*, **31**, 453–463 (1976)

Oğuz, H. N. and A. Prosperetti; "Dynamics of Bubble Growth and Detachment from a Needle," *J. Fluid Mech.*, **257**, 111–145 (1993)

Räbiger, N. and A. Vogelpohl; "Bubble Formation in Stagnant and Flowing Newtonian Liquids," *Ger. Chem. Eng.*, **5**, 314–323 (1982)

Ramakrishnan, S., R. Kumar and N. R. Kuloor; "Studies in Bubble Formation-I Bubble Formation under Constant Flow Conditions," *Chem. Eng. Sci.*, **24**, 731–748 (1969)

Sada, E., A. Yasunishi, S. Katoh and M. Nishioka; "Bubble Formation in Flowing Liquid," *Can. J. Chem. Eng.*, **56**, 669–672 (1978)

Takahashi, T. and T. Miyahara; "Bubble Volume Formed at Submerged Nozzles: Constant Flow Condition," *Kagaku Kogaku Ronbunshu*, **2**, 138–143 (1976)

Takahashi, T., T. Miyahara, S. Senzai and H. Terakado; "Bubble Formation at Submerged Nozzle in Cocurrent, Countercurrent and Crosscurrent Flow," *Kagaku Kogaku Ronbunshu*, **6**, 563–569 (1980)

Tan, R. B. H. and I. J. Harris; "A Model for Non-Spherical Bubble Growth at a Single Orifice," *Chem. Eng. Sci.*, **41**, 3175–3182 (1986)

Tan, R. B. H., W. B. Chen and K. H. Tan; "A Non-Spherical Model for Bubble Formation with Liquid Cross-Flow," *Chem. Eng. Sci.*, **55**, 6259–6267 (2000)

Terasaka, K. and H. Tsuge; "Bubble Formation at a Single Orifice in Highly Viscous Liquids," *J. Chem. Eng. Japan*, **23**, 160–165 (1990)

Terasaka, K., H. Tsuge and H. Matsue; "Bubble Formation in Cocurrently upward Flowing Liquid," *Can. J. Chem. Eng.*, **77**, 458–464 (1999)